

## ARTICLES

**Unique characteristics of cold cathode carbon-nanotube-matrix field emitters**

Philip G. Collins and A. Zettl

*Department of Physics, University of California at Berkeley, Berkeley, California 94720  
and Materials Sciences Division, Lawrence Berkeley National Laboratory, Berkeley, California 94720*

(Received 28 October 1996)

The attributes of electron field emission from disordered matrix arrays of carbon nanotubes are studied and found to be quite reproducible in spite of the disorder, density, and quality variations from sample to sample. At low applied electric fields, the electron field emission current-voltage characteristics qualitatively follow conventional Fowler-Nordheim behavior up to a critical current density. However, the current rise at low applied fields is anomalously steep, suggesting that the Fowler-Nordheim model is not sufficient to quantitatively characterize the emission. In the high-field region, the emission characteristics have a more complex behavior. In that regime, the instantaneous field emission is reminiscent of the low-field behavior, but discrete switching events lead to an overall current suppression. We attribute the sudden and well-defined onset of the switching events to interactions between neighboring nanotube tips. By correlating the switching behavior to the current-voltage characteristics, we rule out other physical processes that cause similar effects.

[S0163-1829(97)09015-2]

**I. INTRODUCTION**

A broad range of electrical, chemical, and mechanical applications can be proposed for carbon nanotubes.<sup>1</sup> But to date the wide range of properties available in these nanoscale building blocks have hindered as much as helped potential applications. For example, the electrical properties of carbon nanotubes are predicted to vary over a wide range, depending sensitively on the tube chirality and diameter.<sup>2,3</sup> Any given multiwall nanotube is a complicated combination of concentric individual tubes, each with different properties. Such complexities greatly hamper the theoretical modeling and experimental characterization of carbon nanotubes. The additional restrictions encountered in manipulating and measuring the properties of nanoscale objects further complicate the characterization and application of carbon nanotubes.

To fully characterize and utilize carbon nanotubes, three pathways are available. In the first, measurements and applications rely on using individual nanotubes, one at a time. Recent progress on this front includes the measurement of structural and mechanical properties of a single nanotube by transmission electron microscopy<sup>4,5</sup> (TEM) and electrical transport measurements aided by microfabrication.<sup>6</sup> A second possible pathway requires adapting the synthesis of nanotubes to produce macroscopic amounts of tubes with uniform properties. Some progress has been made using laser vaporization techniques which yield ‘ropes’ of single-walled nanotubes, where each rope apparently contains a large fraction of nanotubes with similar diameter and chirality.<sup>7</sup> However, this process does not allow for specification from among the many possible nanotube geometries, limiting the potential of nanotubes as, for example, chemical filters for molecules of different sizes. The third pathway to characterization and application involves using, without preselection, as-grown nanotubes with a gross distribution of properties. In this case, selective characterization may still

occur if only a small number of self-selected, similar nanotubes are active during any particular process or measurement.

An example of a self-selective process is the field emission of electrons from carbon nanotube tips.<sup>8,9</sup> A negatively biased nanotube tip, with its nanometer-sized radius of curvature and large aspect ratio, can generate such large, local electric fields that it emits electrons into the vacuum level. We have shown previously<sup>10</sup> that a reliable, robust electron beam source can be made from a disordered collection of field-emitting carbon nanotubes, regardless of the overall distribution of tube geometries. The process is self-selective because only the sharpest protrusions produce local fields large enough to generate field emission. Thus nanotube field emission sharply discriminates between the many tube geometries available in favor of only the sharpest nanotubes; as a result, the emission characteristics reflect only a particular type of nanotube and are quite reproducible.

This paper describes the details of carbon nanotube field-emission characteristics. We find that nanotube field-emission characteristics are extremely predictable, with only small but interesting deviations due to local effects. Two exponential emission current regimes are cleanly separated at a particular universal value of the emission current. The overall field-emission characteristics of the nanotubes are significantly different from those of conventional field emitters.

This paper is organized as follows. First, we provide a description of our experimental procedures. This includes the production of simple nanotube field emission sources and measurement of their current-voltage characteristics. The analysis of these characteristics is then divided into three sections. In Sec. III A, we consider the uniformity of emission properties found for these samples. In Sec. III B, the characteristics are compared to and contrasted with the conventional Fowler-Nordheim model for electron field emission. Various extension models are also considered to fully account for the observed data. In Sec. III C, we discuss evi-

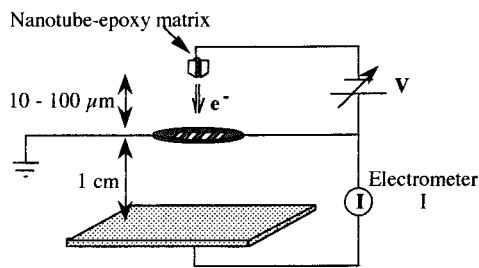


FIG. 1. Schematic of the carbon nanotube field emission experimental setup. The nanotube emission source, acceleration grid, and collector plate are housed in a vacuum chamber at  $10^{-6}$  torr. An electrometer detects the portion of the emission current transmitted through the grid.

dence for tip-tip interactions in the context of emission site switching and conditioning effects.

## II. EXPERIMENT

Multiwall carbon nanotube field emission sources were prepared as follows. Nanotube-containing soot generated from a carbon plasma arc discharge<sup>11</sup> was first burned in flowing oxygen at  $750^\circ\text{C}$  to remove amorphous material. Characterization by TEM revealed that nanotubes typically made up 70% of the remaining material.<sup>5</sup> Tube lengths ranged from stublike growths of a few hundred nanometers in length to fibers  $10\ \mu\text{m}$  and longer which could not be fully imaged within the TEM field of view. Tube diameters spanned a range from 2 to 50 nm. High-resolution TEM inspection of the tubes revealed that many of the tube ends are tapered, with ultimate tip radii of curvature  $R_{\text{tip}}$  smaller than the distribution of tube diameters would suggest. The sharpest tips, which are most likely to act as emitters, were observed to have tip radii of curvature between 1 and 3 nm.

The tube-rich material was thoroughly mixed into non-conducting epoxy in a volume ratio of approximately 1:1 to produce a conductive matrix of nanotubes. Within the matrix the bundles of tubes are completely disordered, with a small fraction of the tubes extending their tips beyond the epoxy at the sample surface. Scanning electron microscopy (SEM) resolved bundles of tubes sticking out from these surfaces in all directions with densities no less than 1 per  $\mu\text{m}^2$ . The nanotube density was sufficient to generate large and reproducible emission currents.

A well-defined emission surface was produced by drying the nanotube-filled epoxy under pressure between two glass slides spaced  $50\ \mu\text{m}$  apart. At the glass slide edges, the excess was removed to leave a uniform  $50\text{-}\mu\text{m}$ -wide stripe of the nanotube-epoxy matrix. The glass-epoxy sandwich was then further mechanically shaped to produce a  $50\times 50\ \mu\text{m}^2$  emission surface of the nanotube-epoxy matrix. Emission currents were always detected from these surfaces, even after significant surface damage, because of the uniform distribution of sharp tips throughout the epoxy matrix. Even harsh mechanical sanding or “burning” of the matrix surface by high-voltage arcing simply exposed new tube tips from the underlying matrix to serve as fresh emission sources.

Figure 1 depicts the experimental setup for detecting nanotube field emission. The samples were placed in a

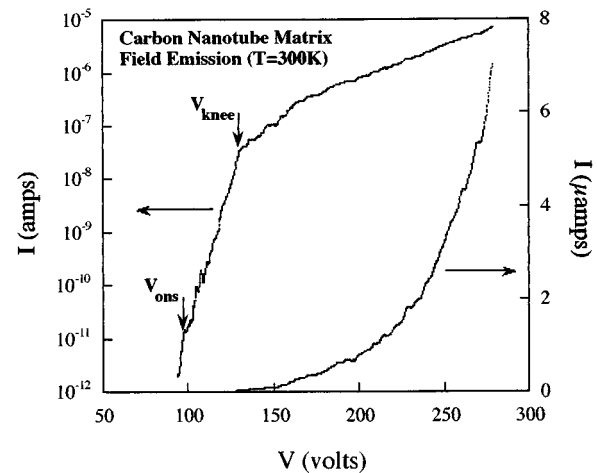


FIG. 2.  $I$ - $V$  curve for field emission from carbon-nanotube-matrix sample, showing both logarithmic and linear current scales.

vacuum chamber at  $10^{-6}$  Torr. Using a precision micrometer, the prepared surfaces were brought into contact with a 50% transmitting copper grid and then withdrawn by  $10\text{--}100\ \mu\text{m}$  from the grid. The samples were then biased at high negative voltage  $V$  with respect to the grounded grid. Electrons field emitted from the sample surface were accelerated by this bias towards the grid. Roughly half of the total emitted electrons passed through the grid and were collected onto a copper plate and detected as a current  $I$ , using a well-isolated electrometer. Under computer control, the voltage bias could be ramped in 70 mV increments. For all of the data presented here, the sample matrix temperature was maintained at  $T=300\ \text{K}$ , hence the emission characteristics are for a cold-cathode configuration.

Temporal resolution of the emission current was limited by the 1 kHz output bandwidth of the electrometer. In practice, the emission current was averaged for up to 1 sec at each voltage value. Averaging the current produces the smoothest curves and is a useful tool for describing the overall behavior of the nanotube field emission. However, such averaging filters out fluctuations in the emission current. The collection of multiple independent current readings at a single voltage bias proved to be as illuminating as the smooth, time-averaged curves, and allowed for a better understanding of these samples. Both types of measurement results are analyzed below. In Secs. III A and III B, the characteristics of the smoothly varying, time-averaged curves are examined. In Sec. III C, the time-varying component of the emission is explored. This additional temporal component is critical for understanding the emission properties of carbon nanotubes in the high electric-field regime.

## III. RESULTS AND DISCUSSION

### A. Field emission onset and nanotube tip dependence

Figure 2 shows a typical current-voltage ( $I$ - $V$ ) characteristic of a nanotube-matrix field emitter with current on both logarithmic and linear scales. The sample-grid separation is  $d=50\ \mu\text{m}$ . The onset voltage  $V_{\text{ons}}$ , which typically occurs near 100 V, is arbitrarily defined as the bias for which a 10-pA emission current is measured. Above  $V_{\text{ons}}$  there are

two exponential regimes, as clearly seen in the logarithmically plotted data. A knee voltage  $V_{\text{knee}}$  is defined as the breakpoint at which the emission data deviate from the low-voltage, straight-line asymptote. For the sample used for Fig. 2, values of  $V_{\text{ons}}$  and  $V_{\text{knee}}$  are 97 and 130 V, respectively.

For a sample surface separated from the accelerating grid by  $50 \mu\text{m}$ , these voltages suggest average electric fields on the order of  $10^4 \text{ V/cm}$  if we assume the two planar electrodes have a uniform field between them. However,  $10^4 \text{ V/cm}$  is approximately three orders of magnitude lower than the characteristic onset field required for field emission into vacuum.<sup>12</sup> In addition, we find that the nanotube emission characteristics are relatively insensitive to variations in the sample-grid separation. Varying this distance from 10 to  $100 \mu\text{m}$  results in only a 10% increase in the observed  $V_{\text{ons}}$  (and a corresponding shift of the  $I$ - $V$  curve). The emission characteristics remain essentially unchanged even when the average field varies by an order of magnitude. Thus we conclude that a planar electrode model, as suggested by our physical setup, is wholly inappropriate for the nanotube emitters.

The low onset voltage and insensitivity to sample-grid separation  $d$  both suggest that a local electric-field model is more suitable. In this case, the electric-field concentration at the emitting nanotube tips is primarily an effect of the nanoscale tip geometry and the tip's immediate environment. The nanotube tip, which is typically within  $1 \mu\text{m}$  of the emitter surface, is at the same potential as the surface but concentrates the electric field due to the small radius of curvature. Accordingly, we may model each tip as a hemisphere<sup>12,13</sup> with a local field

$$E_{\text{loc}} = V_{\text{applied}} / (\alpha R_{\text{tip}}), \quad (1)$$

where  $R_{\text{tip}}$  is the tip radius of curvature and  $\alpha$  is a modifying factor determined by local geometric and electronic factors. Using a characteristic value of  $R_{\text{tip}} \approx 1 \text{ nm}$  as observed by TEM and a "typical" emission electric field of  $E_{\text{loc}} \approx 10^8 \text{ V/cm}$ , we find  $\alpha$  to be on the order of 10. Theoretically, an  $\alpha$  between 3 and 5 can result solely from the screening due to image charges.<sup>12</sup> In our case  $\alpha$  also includes the effects of screening by nearby protrusions, including the nonemitting nanotubes, and the not-so-distant epoxy matrix. In addition,  $\alpha$  may include electronic effects of the presumably low-dimensional nanotubes. Therefore a value of  $\alpha \approx 10$  is not unreasonable for the nanotube emitters, and the small observed onset voltage and relative insensitivity to  $d$  can be explained without invoking novel emission mechanisms or any other "magnification" factors.

The simplicity of the isolated hemisphere model allows us to argue that only the sharpest tips in the nanotube matrix are active in our measurements. The electron emission current depends exponentially on the local electric field  $E_{\text{loc}}$ . By Eq. (1), then, the emission depends exponentially on the nanotube tip radius  $R_{\text{tip}}$  and only the sharpest tips can emit at low applied voltages. As the voltage is increased, the exponentially rising current from these active tips conceals the turn-on events of larger radius tips, if any turn on at all. In this sense the emission process itself self-selects among the broad distribution of nanotube properties, so that only the narrowest tubes, independent of length, are represented in the data. We have tested this hypothesis by measuring field

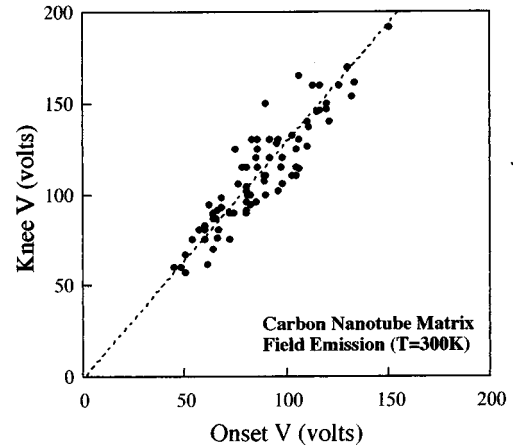


FIG. 3. Knee voltage as a function of onset voltage for a variety of nanotube emission samples. The dashed line is a straight-line fit with slope  $1.29 \pm 0.08$  passing through the origin. The correspondence indicates that, corrected for local geometries, the nanotube emitters have a single, well-defined breakpoint.

emission from samples made of monodisperse single-walled tubes with  $R_{\text{tip}} = 1 \text{ nm}$  and find results identical to Fig. 2 for all samples.<sup>14</sup> Thus the experimentally measured field emission is completely insensitive to the broad range of tip geometries present in the sample.

Figure 3 depicts the range of observed voltages  $V_{\text{ons}}$  and  $V_{\text{knee}}$  for many different samples prepared by similar methods and measured at room temperature. The observed range in onset voltage  $V_{\text{ons}}$  is to be expected, and can almost exclusively be considered an effect of the local geometry surrounding each nanotube. Surprisingly, every one of these samples shows a breakpoint  $V_{\text{knee}}$  in its  $I$ - $V$  characteristic. By plotting  $V_{\text{knee}}$  against  $V_{\text{ons}}$  for each sample as is done in Fig. 3, a clear and surprising correspondence is revealed. The straight-line fit in Fig. 3 indicates  $V_{\text{knee}} = (1.29 \pm 0.08) V_{\text{ons}}$  for the entire ensemble of nanotube-matrix emitters. The fit indicates that variations in  $V_{\text{knee}}$  for different nanotube matrix samples are only due to the same local variability as for  $V_{\text{ons}}$ . We may argue, then, that the local electric fields associated with the onset and with the breakpoint are well-defined constants for the selected class of field-emitting nanotubes (i.e., those with the sharpest tips).

Having characterized the local electric field at the nanotube tip, we next turn our attention to the local tip emission current density, which is a more difficult quantity to accurately determine. The experimentally measured current  $I$  is only a fraction (on the order of one-half) of the total electron beam, since many of the emitted electrons are captured by the accelerating grid before reaching the collector plate. Furthermore, the sample-grid spacing in this study is nearly the same size as the opaque stripes of the grid, which are approximately  $100 \mu\text{m}$  wide. Therefore, if the emission is from only a few sites on the surface, the measured current at the collector will depend strongly on the relative positioning of these sites with respect to the grid. Due to the small size of the emission samples, it is difficult to quantitatively determine how many independent emission sites are active on the surface. However, two facts seem to indicate that the emission is, on a gross scale, uniform across the surface. First, we find surprisingly little matrix sample-to-sample variation.

The reproducibility of the measured collector current from one sample to the next is almost anomalously consistent considering the disordered nature of the nanotube matrix surfaces. Second, as previously mentioned, the emission current is found to depend only weakly on the sample-grid separation. Due to the experimental setup, changing the perpendicular sample-grid separation invariably causes parallel translational motion between the grid and sample surface. If only a few strongly emitting sites dominated the total current, the combined perpendicular and parallel motions would be expected to lead to sizable variations in the measured emission current, contrary to experimental observations. We therefore assume that a large fraction of the sample surface is uniformly active, at least on the micrometer length scale. In order to calculate a lower bound on the local tip emission current density, we shall below assume that the entire surface emits uniformly.

Two current density values of particular interest are the maximum attainable current density and the current density at the breakpoint  $V_{\text{knee}}$ . The maximum current in Fig. 2 is  $I=8\ \mu\text{A}$ , suggestive of a total field-emission current from the matrix surface of  $16\ \mu\text{A}$  after accounting for the shielding of the accelerating grid. Thus, as an absolute minimum, this matrix sample is capable of supporting a total surface current density on the order of  $600\ \text{mA}/\text{cm}^2$ . To calculate a tip current density, we make the conservative assumptions that every tube emits equally and that the active emission surface per tip is  $4\pi R_{\text{tip}}^2$ . From the SEM observation of on average one tube per square micrometer, we calculate for this sample a maximum current of  $6\ \text{nA}$  per nanotube and a tip current density of  $5\times 10^4\ \text{A}/\text{cm}^2$ . The second current density of interest is the critical current at the breakpoint of the  $I$ - $V$  characteristic. In Fig. 2, the emission current  $I$  at  $V_{\text{knee}}$  is  $35\ \text{nA}$ , corresponding to a total matrix surface emission current density  $J=3\ \text{mA}/\text{cm}^2$ . This value implies a minimum current of  $30\ \text{pA}$  per nanotube and a tip current density of  $200\ \text{A}/\text{cm}^2$ .

The maximum sample emission current varies from  $1$  to  $50\ \mu\text{A}$  from sample to sample, perhaps indicating a variation in the number of emitting nanotubes. However, the measured emission current at  $V_{\text{knee}}$  is relatively predictable for these matrix samples. We find this value to be a universal constant  $I_{\text{knee}}=20\pm 15\ \text{nA}$  for *all* nanotube emission samples, with the large error bars due to the steepness of the current rise at this voltage. This constant current value and the behavior of  $V_{\text{knee}}$  demonstrated in Fig. 3 uniquely determine a single point on the  $I$ - $V$  characteristic at  $(V_{\text{knee}}, I_{\text{knee}})=(1.29 V_{\text{ons}}, 20\ \text{nA})$  which all of our  $50\times 50\ \mu\text{m}^2$  nanotube matrix samples appear to meet. This result is quite unexpected for a number of reasons. Little care was taken to prepare quality surfaces which would give sample-to-sample reproducibility, aside from the similar surface areas. Also, the likely distribution of potential nanotube emitters on each surface is broad. Finally, the density of nanotube material in each sample may vary over as much as an order of magnitude due to variations in the quantity of epoxy mixed into the nanotube-containing soot. All of these reasons support the wide range of maximum sample emission currents, but apparently contradict the constant value of  $I_{\text{knee}}$ . The single, well-defined breakpoint common among all measurements is more reminiscent of a carefully prepared semiconductor crystal facet<sup>15</sup> than the relatively inhomogeneous matrix samples described here.

We concern ourselves below with possible causes of this unexpected, but reproducible and potentially very useful, feature.

### B. Modeling field-emission current behavior

The well-defined breakpoint at  $(V_{\text{knee}}, I_{\text{knee}})$  confirms that emission is very selective among the various nanotubes protruding from the matrix sample. It is also suggestive of a common physical property among these particular tubes, for example, a current saturation limit. In order to investigate further the breakpoint at  $V_{\text{knee}}$ , additional analysis of the  $I$ - $V$  characteristic is helpful.

Conventional field-emission analysis utilizes the model of Fowler and Nordheim,<sup>16</sup> which was originally developed for individual, isolated, noble-metal tips emitting into vacuum. Subsequent experiments have shown the Fowler-Nordheim (FN) model to be widely applicable to many emitting systems.<sup>17</sup> The recent nanotube electrical conductivity measurements of Langer *et al.*<sup>6</sup> indicate that multiwalled carbon nanotubes are metallic, at least at room temperature. Therefore, the FN model could be reasonably expected to apply to nanotube matrix field-emission characteristics.

In the FN model, the electron current density  $J$  at the emitting tip can be calculated as a function of the local electric field  $E_{\text{loc}}$  and the tip work function  $\Phi$ . The resulting FN equation is

$$J \propto E_{\text{loc}}^2 \exp[-6.8 \times 10^7 \Phi^{3/2}/E_{\text{loc}}], \quad (2)$$

where  $E$  is in units of  $\text{V}/\text{cm}$ ,  $\Phi$  in units of  $\text{eV}$ , and  $J$  in units of  $\text{A}/\text{cm}^2$ . Assuming the isolated hemisphere model for  $E_{\text{loc}}$  given by Eq. (1), the FN equation may be rearranged in terms of experimentally measured quantities such as the total current  $I$  and applied voltage  $V$  measured in  $\text{A}$  and  $\text{V}$  to give

$$\ln\left(\frac{I}{V^2}\right) = \frac{1}{V} (-6.8\alpha R_{\text{tip}}\Phi^{3/2}) + \text{offset}, \quad (3)$$

with  $R_{\text{tip}}$  measured in  $\text{nm}$ . For small excursions in applied voltage, the logarithmic behavior dominates the emission  $I$ - $V$  characteristic and the quantity  $(\alpha R_{\text{tip}}\Phi^{3/2})$  may be determined from experimental data.

Figure 4 is a Fowler-Nordheim plot of  $\ln(I/V^2)$  against  $1/V$  for the emission data of Fig. 2. For a conventional field emitter, this plot results in a straight line with slope  $-6.8$  ( $\alpha R_{\text{tip}}\Phi^{3/2}$ ). The two regimes above and below  $V_{\text{knee}}$  in Fig. 4 both appear to fit this Fowler-Nordheim criterion, but give quite different slopes.

In the low-voltage region, the best-fit slope for the data is  $S_{\text{LV}}=-2700$ . Assuming values of  $R_{\text{tip}}=1\ \text{nm}$  and  $\alpha\approx 10$ , this slope gives  $\Phi=12\ \text{eV}$ . This work function is unphysically large, and no reasonable adjustments of other parameters can bring  $\Phi$  into a more realistic range. Furthermore, as described in Sec. III A, we observe two uniquely defined points on the  $I$ - $V$  characteristics for all of our samples. One of the points is the onset, defined at  $(V_{\text{ons}}, 10\ \text{pA})$ . The other is the breakpoint at  $(V_{\text{knee}}, I_{\text{knee}})=(1.29V_{\text{ons}}, 20\ \text{nA})$ . These two points alone can be used to calculate a low-voltage ‘FN slope’ without any foreknowledge of  $\alpha$ ,  $\Phi$ , or the tip radius  $R_{\text{tip}}$ . That calculation yields a value  $S=-3100$ , quite close to the value obtained from the low-voltage regime of Fig. 4.

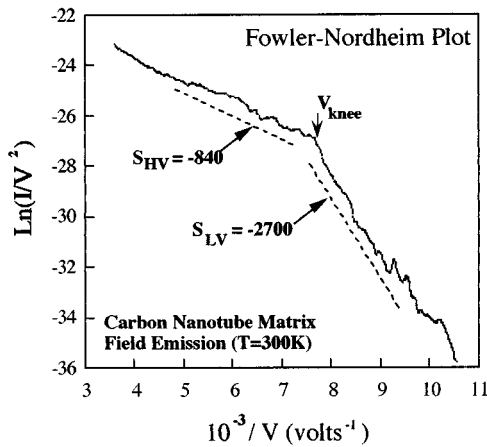


FIG. 4. Fowler-Nordheim plot of  $\ln(I/V^2)$  versus  $1/V$  for a nanotube matrix sample. For conventional field-emission tips, such a plot results in a straight line. The nanotube data fit the Fowler-Nordheim equation well in both the high voltage (HV) and low voltage (LV) regions. However the interpretation of the Fowler-Nordheim slopes (indicated by dashed lines) is more complex than for the case of conventional field emission sources (see text).

This agreement and the unlikely value  $\Phi = 12$  eV suggested by it indicate that the FN equation fails to accurately model these emitters, at least for low fields below  $V_{\text{knee}}$ . In physical terms, the current rises far too fast as a function of voltage to be explained by conventional electron emission into the vacuum for the carbon nanotube matrix emitters.

In the high-voltage region above  $V_{\text{knee}}$  the data of Fig. 4 also give a straight-line fit but with slope  $S_{\text{HV}} = -840$ . Again assuming  $R_{\text{tip}} = 1$  nm and  $\alpha \approx 10$ , this value gives a tip work function of  $\Phi = 5.4$  eV, in agreement with the 5 eV work function of graphite. However, unlike the low-voltage slope, the sample-to-sample spread in  $S_{\text{HV}}$  is quite broad, leading to variations in the calculated  $\Phi$  from 2.7 to 8.2 eV. This variation, in combination with the failure of the FN model at low voltages, makes the evaluation of  $\Phi$  from Eq. (3) unreliable even in this field regime.

A failure of the FN model in describing conventional field emitters is often accounted for by the incorporation of additional interactions. The theory of Dyke and Dolan<sup>18</sup> includes the effects of vacuum space charge surrounding an emission site. At high-current densities, this space charge sharply reduces the actual electric field at the emitter. The FN linearity criterion will fail when the space charge becomes significant because the local electric field is no longer proportional to the applied voltage. Saturation of the emitter current due to limited carrier concentration in a nonmetallic emitter can add to or exaggerate this space-charge effect.<sup>17,19</sup>

The combination of space-charge buildup and carrier saturation explains the sharp breakpoints observed in the field-emission characteristics of semiconductors.<sup>15,19</sup> We note this example because, at first sight, the nanotube results reported here exactly match the field-emission characteristics of semiconductor crystal facets. The important difference is that the semiconductors follow standard FN behavior up to a particular field, and then deviate. At higher fields, the current gradually saturates to a point at which it no longer increases. Both of these rules are broken in the case of nanotube emitters. As described above, the FN model fares worst for nano-

tube emitters in the low-field regime, even though space-charge effects should be insignificant. Furthermore, in the high-field regime the current continues to rise smoothly and exponentially over no less than two orders of magnitude. We therefore rule out space charge or low carrier density as a cause of the field-emission breakpoint in nanotubes. For the same reasons, accounting for the resistivity of the substrate or of the nanotubes themselves cannot bring the experimental data into accord with the predictions of a conventional FN model.

The FN model may not apply well to the nanotube samples for a variety of reasons. First of all, the nanotube tips may have localized electronic states only weakly coupled to the bulk of the tube. In the FN model, such states are assumed to be in equilibrium with the essentially infinite reservoirs associated with good metals. Second, the FN model assumes a single emitter, completely independent of its surroundings. In using the FN model, we have ignored the effects of multiple emitting nanotubes, other nonemitting but nevertheless sharp nanotubes nearby, and the epoxy matrix stabilizing these tubes. Section III A described the sample-to-sample uniformity of emission and concluded that the emission does not simply behave as emission from a very small number of discrete protruding tips, since the emission appears relatively uniform over a scale of many micrometers. The FN model does not include any interactions which, in these nanotube matrix samples, may play an important role in spatially “homogenizing” the emission-current density. For example, the emission current might be stabilized and spatially averaged by cooperative effects between the many tubes. A cooperative interaction between tips could explain both the spatial uniformity of the emission current as well as the anomalously steep current rise of low fields, neither of which fit in the FN model. The emission current might also be influenced by the surrounding environment. Additional sharp nanotubes lie both above and just below the surface of the epoxy matrix and produce large electric fields of their own. The entire configuration of tips may create a complex field distribution beyond the standard FN model.

Nanotube tips just below the surface of the epoxy not only redistribute the local fields, but may be field emitters as well. Field emission has been observed for conducting particles *below* the surface of a nonconductive matrix.<sup>20,21</sup> In the presence of very large electric fields, the electronic bands of the insulating matrix may be significantly modified, even to the point of dielectric breakdown and transport through the insulator. In our nanotube matrix samples, nanotube tips that do not protrude from the surface, but are close to it, could cause such effects. In that case the emission is not simply a matter of tunneling into the vacuum from a nanotube tip; rather, the tip induces a large enough field to cause dielectric breakdown and emission from the insulator into the vacuum.

This unique mode of field emission has been theoretically modeled by Latham and Wilson.<sup>22</sup> In the model of Latham and Wilson, the electronic properties of the insulating layer, as opposed to the emitters themselves, dominate the  $I$ - $V$  characteristics of the emission. Three aspects of the model of Latham and Wilson suggest that, at least in the low-field regime below  $V_{\text{knee}}$ , it may apply to the nanotube-matrix samples better than the FN model. First, the Latham model predicts a very sharp turn-on event as we have observed. At

the onset of field emission from metallic tips, some electrons must tunnel through the insulator to reach vacuum. This tunnel current within the epoxy can lead to a local dielectric breakdown and a current avalanche. Second, the model of Latham and Wilson provides for electron emission at lower applied fields than the standard FN model. This effect is due to a concentration of field by the high dielectric constant  $\epsilon$  of the insulating material. The barely submerged nanotube tip surrounded by a large  $\epsilon$  will experience a larger local field than the nearby tip protruding into the vacuum space. Dielectric breakdown may also excite holes in the insulator, which will diffuse toward the emitting tip and produce an “inverse” space charge that further increases the local electric field. Both effects increase the local field at an emitting tip and would account for the strong emission currents measured from the nanotubes at relatively small local fields. The third attractive feature of the model of Latham and Wilson is its formulation, which results in the same functional form as the FN equation [Eq. (3)]. Therefore the linearity of the nanotube data, when plotted as in Fig. 4, merely confirms that *either* the model of Fowler Nordheim or Latham and Wilson applies to these emitters. For the model of Latham and Wilson, the slope of the FN plot is given<sup>22</sup> by

$$S = -1.5\epsilon\chi(d/\Delta), \quad (4)$$

where  $\chi$  is the work function of the insulator-vacuum interface measured in eV,  $d$  is the sample-to-grid separation, and  $\Delta$  is the thickness of the insulating layer. For typical values of  $\epsilon \approx 10$  and  $\chi \approx 7$  eV for an insulator, the observed low-voltage slope  $S_{LV} = -3000$  from Fig. 3 suggests an insulating layer thickness  $\Delta = 0.5 \mu\text{m}$ . Though difficult to experimentally confirm, this reasonable value for  $\Delta$  indicates that Eq. (4) may qualitatively describe the observed emission characteristic. However, Eq. (4) predicts a proportional relationship between the slope  $S$  and the sample-grid separation  $d$ . As described in Sec. III A, we do not observe any marked dependence on the sample-grid separation. It is unclear whether the isolated hemisphere model for the nanotube tips, as described in Sec. III A, could be incorporated into the surface-sensitive model of Latham and Wilson.

Presumably, field emission may be measured for nanotube-matrix samples in which no nanotubes actually protrude beyond the epoxy surface. Although this is not the case for our samples, it indicates one way that the field emission can be far more complicated than the conventional FN model. An accurate model of the field emission for these nanotube-matrix samples would likely incorporate four interdependent elements: (1) the emission from the extended, bare nanotube tips, (2) the insulator-assisted emission of nanotube tips just below the epoxy surface, (3) a self-consistent distribution of electric fields concentrated by each nanotube tip, and (4) the dynamic effects of current flow by which emitting tips may interfere or cooperate with each other. All four aspects are subordinate to the self-selection of the sharpest nanotube tips already described. Among these tips, however, there is a possibility for correlations due to the electric fields and currents. Further theoretical analysis may be required to illuminate which process dominates the emission characteristics of the carbon nanotube matrices.

Within any proposed framework, the high field-emission characteristics, including the  $I$ - $V$  breakpoint at  $V_{\text{knee}}$ , remain

unexplained. We first consider the possibility that, independent of the process for the emission, a structural modification is causing the observed effect. Stress from the large electric fields combined with Joule heating might cause a structural or electronic rearrangement of a nanotube tip, which in turn would change features in the tip's emission. Previous work<sup>8</sup> has correlated increases in nanotube field-emission currents with laser-induced tip modification. The conclusion was reached that nanotube emission changed after a laser-induced structural unraveling, which resulted in an ultrasharp, single-atom protrusion. The present work covers the same electric field and current density regime, but no evidence of tip modification is observed. For example, modification of the tip should change both the slope of the FN plot and the magnitude of the observed emission current. Although we observe the former, we observe no discontinuities in the emission current near  $V_{\text{knee}}$ . In fact, the  $I$ - $V$  characteristics reported here show no hysteresis upon repeatedly increasing and decreasing the applied bias through the observed breakpoint. Therefore the local structure governing the emission can at most be slowly varying in our work. We rule out the possibility that by going to higher fields we have caused the same effects previously reported for laser irradiation of the nanotube tip.

We have further tested this conclusion by completing parallel studies of field emission from microcrystalline graphite. The electronic structure of multiwalled carbon nanotubes is predicted to be very similar to graphite.<sup>23</sup> When observed edge on, a graphite crystal protruding from an epoxy surface matches a protruding nanotube in geometry and, more importantly, in atomic structure. Given these similarities, both materials might be expected to unravel or form dangling bonds under equivalent conditions. We prepared matrix samples using pure graphite rather than the nanotube-rich carbon soot, but otherwise made no changes to our procedures. We find the graphite-matrix samples to be field emitters with onset voltages between 150 and 300 V. Although two to three times higher than the onset voltages observed for nanotubes, these values suggest local fields on the same order of magnitude as for the carbon nanotubes. Most importantly, the graphite  $I$ - $V$  characteristics show *no* knee or breakpoint up to currents 100 times higher than observed for the nanotubes.

This striking difference between graphite and carbon nanotube emitters has two important implications. First, it confirms that the carbon-carbon bonding is not a source of structural instability. Second, it limits the applicability of the model of Latham and Wilson, which is governed by interaction with insulating material. For a model which only weakly depends on the emitters themselves, dramatic differences should not be found between emitters so similar both structurally and electronically.

### C. Switching and conditioning instabilities

In the preceding analysis, only time-averaged data have been considered. In this section, we also consider the time-dependent fluctuations of the field-emission current. The experimental conditions were not changed except for the removal of a post-acquisition digital filter. First, we consider only the time dependence of the emission current at a fixed voltage bias. Then, we discuss the same time dependence

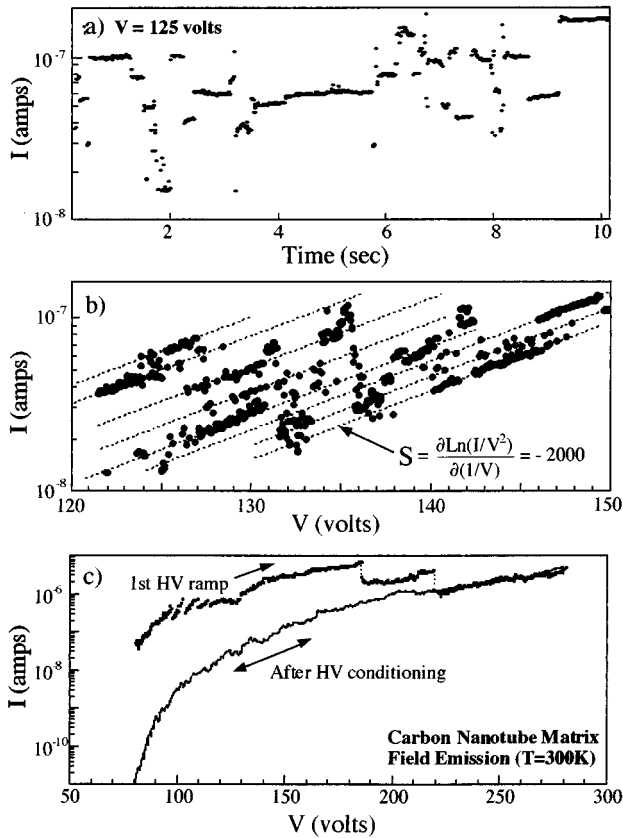


FIG. 5. Emission current versus time (a) and versus voltage (b) show switching transitions between similar emission configurations with nearly the same instantaneous  $I$ - $V$  slope, as depicted by the dotted lines. Some aspect of the switching process leads to the overall decrease in the average slope of the  $I$ - $V$  curve. (c) A conditioning high voltage (HV) ramp on a pristine sample leads to two “events” that remove all evidence of discrete structure in the emission, although the knee still occurs.

while allowing the bias to change. At the end of this section we describe further effects of ramping the sample bias to very high voltages.

### 1. Current switching versus time

Figure 5(a) shows the behavior of a pristine multiwalled nanotube matrix emitter subjected to a constant bias voltage of 125 V, which exceeds  $V_{\text{knee}}=85$  V. With the bias held steady, the current was collected as a function of time. Discrete jumps are apparent in the plot, with similar characteristics to those reported previously for an individual, single-walled carbon nanotube<sup>8</sup> and for other carbon emitters.<sup>24,25</sup>

Typically, this unsteady current behavior is caused by changes in the emitting tip, such as the movement of adsorbates or motion of the emitting facet itself. For example, on a single crystalline tip of a conventional field emitter, each crystal face has a slightly different work function. Electron emission from one face surrounds the entire tip in a dynamic space charge which can shield and preclude the other faces from emitting. For nearly identical faces, the system is metastable and the active emission surface will jump from face to face. As this occurs, the measured current shows small discrete steps or “switching” for the not quite equivalent sites.<sup>17</sup>

Although this explanation describes the switching effects seen for an individual emitter, additional phenomena may occur for arrays of emitters. In the case of the nanotube matrix samples discussed here, we must also consider the possibility of interaction between nanotube tips. The tips are terminated in nearly identical caps of 1 nm radius and, since densely packed, may act as interfering emission sites in the same way that crystal faces do on a single tip conventional emitter. The space charge of one emitting tip may preclude other nearby tips from emitting, until some instability leads to a reconfiguration of the active site or sites. Similar interference can be seen in dense arrays of lithographically created emission sites.<sup>26</sup> A distinction between the two processes is that intratip switching can occur at very low current densities; intertip switching can only occur when the spatial extent of the charging effects becomes comparable to the separation between emission sites. The behavior in Fig. 5(a) could indicate either intertip or intratip switching because it occurs in the high current density regime above  $V_{\text{knee}}$ .

### 2. Current switching versus time and voltage

Figure 5(b) is an  $I$ - $V$  curve obtained in a small region above  $V_{\text{knee}}$  for the same sample as was used in Fig. 5(a). The data acquisition rates of Figs. 5(a) and 5(b) are approximately equal; however in Fig. 5(b) the bias voltage is steadily ramping. The ramping rate has been chosen so that two separate effects can be clearly seen. First, the switching behavior for  $I(t)$  as seen in Fig. 5(a) is still quite apparent, since at each voltage value more than one current value is plotted. In addition, the ramping rate is fast enough that the gradual current rise can be distinguished from the switching noise, allowing measurement of the  $I$ - $V$  characteristic slope.

The switching behavior in  $I(t)$  manifests itself as sloping line segments in the plot of  $I(V)$ . In other words, steady emission configurations which produce horizontal line segments in  $I(t)$  cause tilted line segments in the plot of  $I(V)$  due to the changing bias voltage. As long as the emission configuration is steady, the  $I(V)$  segment should display a characteristic slope as given by either Eq. (3) in the FN model or Eq. (4) in the model of Latham and Wilson. When the emission configuration rearranges, for example, by suppressing certain sites, there is a discrete change in the current magnitude, but then the  $I$ - $V$  curve again rises at the previous rate. The constancy of line segment slopes (as indicated by the dotted lines) in Fig. 5(b) indicates that the switching is between nearly equivalent configurations of emitting sites.

Most importantly, the instantaneous slope (calculated as for a FN plot) of any segment in Fig. 5(b) nearly matches the low-voltage slope  $S_{LV}\approx 3000$  normally found only below  $V_{\text{knee}}$ . The remarkable point is that the emitter character, as quantified by this instantaneous slope, has not changed even though the voltage is above  $V_{\text{knee}}$ . Rather, the instantaneous slope of the  $I$ - $V$  characteristic appears to be a constant both above and below  $V_{\text{knee}}$ . This constancy indicates that the emission itself, when from a single stable emission configuration, does not deviate from its low-voltage behavior. Also, this constancy is further evidence of a stable emitter geometry.

The physical significance of the breakpoint at  $(I_{\text{knee}}, V_{\text{knee}})$  is therefore not a change in the emission character *per se*, nor a breakdown of the emission model, but a turning on

of a current-limiting phenomenon related to the switching behavior. Figure 5(b) clearly depicts the effect of switching on the overall current rise. The voltage range of the figure should result in nearly a 200-fold increase in current, as judged from the slope of any individual data “line segment;” from the actual measurements the total current rises by only a factor of 5. Although the instantaneous slopes of line segments are large, each switching event contributes to the decrease of the overall average slope. If the switching events were not causing this decrease, one would observe the switching fluctuations to be above and below a single line of constant slope.

$V_{\text{knee}}$  is therefore the voltage at which a switching-related current degradation begins to occur. Although not resolved below  $V_{\text{knee}}$ , switching on a smaller scale may occur in that regime as well. We propose that below  $V_{\text{knee}}$ , any switching behavior is only intratip and the tips are noninteracting. Above  $V_{\text{knee}}$ , however, the charging effects at each emitting tip begin to overlap and cause strong intertip switching effects, with consequent modification of the  $I$ - $V$  characteristics. Such a crossover could produce the sharp breakpoint feature observed in the time-averaged data of Fig. 2. It does not, however, explain the current degradation for biases above  $V_{\text{knee}}$ . By some mechanism, the tip-to-tip switching degrades the emitter current so that the average current rise is much less than would be obtained by a single steady emitter.

### 3. Quenching of switching behaviors

Emission current degradation via switching events in the nanotube matrix samples is an important effect that can be easily overlooked for the following reason. Conventional, non-nanotube field emitters that have been exposed to atmosphere commonly require a high-voltage “conditioning” ramp before they exhibit a stable onset field and current response. This is true for our nanotube matrix samples as well, but this high-voltage conditioning also destroys the switching evidence displayed in Figs. 5(a) and 5(b).

Figure 5(c) displays the behavior of a sample before and after ramping to high voltage. At  $V_{\text{knee}}=90$  V, the upper  $I$ - $V$  curve begins to show the switching behavior described above. On an expanded scale as for Fig. 5(b), a discrepancy between average and instantaneous slope can be discerned as the bias rises all the way to 170 V; at higher voltages, the current appears smooth within our experimental resolution. Heating effects due to the increasing current likely cause a gradual increase in the switching rate, resulting in a smaller and smaller switching period as the voltage is increased. Near 185 and 215 V, the tip undergoes two irreversible changes which are most likely nanotube burn-out events. All subsequent  $I$ - $V$  curves have higher, more reproducible  $V_{\text{ons}}$  and  $V_{\text{knee}}$  but no longer show any of the structure in Figs. 5(a) and 5(b). The lower curve in Fig. 5(c) is an example of this later, smoothed characteristic. Moreover, time averaging the current now results in reproducible  $I$ - $V$  characteristics as depicted in Fig. 2. The data of Figs. 2–4 are all for conditioned samples.

After a conditioning cycle, the  $I$ - $V$  breakpoint is still present but discrete structure is no longer resolved. Since the breakpoint is related to discrete switching events, as described above, the switching must still be occurring but at a rate beyond our resolution. An increased rate of switching

would also explain the smoother, more reproducible curves we obtain, since the recorded current is now an averaged emission from many active sites. Earlier studies have seen similar switching and conditioning effects on other nonmetallic emission sites.<sup>27</sup>

Why does the conditioning ramp lead to a higher onset voltage and a faster switching rate? A possible explanation is that the lowest-onset field emitters burn out and are replaced by other, more stable emitters with higher-onset voltages. In a pristine sample, the stable emission configurations may be dominated by the nanotubes protruding furthest from the surface, which are the least screened and will have the lowest onsets. These tips exist in small numbers and the switching between configurations of them will occur slowly enough to be resolved, as in Fig. 5(a). These nanotubes, though, are also most likely to suffer damage from large local fields. After conditioning, these extended nanotubes have been burned or broken off, resulting in a more uniform stubble of tube ends equally shielded and supported by the nearby substrate. The increase in potential emission sites results in many more equivalent emission configurations, such that switching may now occur quite rapidly. We note that the shortened nanotubes retain the same diameter and radius of curvature at their tips, so that conditioning does not necessarily change the slope of the  $I$ - $V$  characteristic.

After conditioning, the nanotube  $I$ - $V$  characteristics appear similar to other field-emitting systems, most notably semiconductor field emitters and nanostructured W tips.<sup>28</sup> In these two systems, as in the nanotube case, electronic localization on the tips or in the low-dimensional region between tip and base can limit the electron emission, resulting in experimentally observable current saturation. In this paper, however, the nanotube emission current rises smoothly and exponentially for three orders of magnitude past the breakpoint at  $V_{\text{knee}}$ . An electronic localization argument, therefore, may not explain the behavior which we have attributed to intertip switching. On the contrary, our comparison between nanotubes and microcrystalline graphite particles suggests the dimensionality to be critical. The differences between the nanotube and graphite systems lead to a reproducible breakpoint in one system but not the other. The observed difference between the two systems may be solely determined by nanotube’s reduced dimensionality and resultant electronic effects. Possibly the nanotubes, which confine the current to a smaller area than the graphite particles, are more susceptible to resistive heating.<sup>29</sup> The observed  $I$ - $V$  characteristics could be the effect of a complicated cooperative process in which each nanotube tip emits, heats, saturates, turns off, cools down, and then emits again. In any case, the breakpoint in the nanotube system but not the graphite system is indicative of an effect that depends on the particular properties of the nanotubes themselves.

## IV. CONCLUSION

Cold cathode carbon-nanotube field emitters have been shown to have very reproducible current characteristics that, though similar to some systems, are quite unique. The reproducibility alone indicates that the active emitting nanotubes are far more uniform than the initial starting materials. With a simple physical picture, we have argued that only a specific

class of nanotubes is active in the emission process.

We have also demonstrated that these emitters turn on too quickly to be considered conventional, independent Fowler Nordheim emitters. In the latter portion of the paper, evidence was found for strong intertip coupling. This coupling causes the well-defined breakpoint in the current-voltage characteristics of the emitters and may lead to the sharp turn on at low electric fields. Fine structure in the characteristics of pristine samples allows us to attribute the breakpoint to switching between different configurations of active tips, as opposed to the tip electron emission itself. We have proposed simple physical explanations for the switching and for the disappearance of the fine structure after high-voltage conditioning.

The unique behavior of these nanotube matrix field emitters may be exploited by various electronic applications. The current-voltage characteristics are very reproducible, with easily distinguishable “on” and “off” regimes and a short, sharp transition region. In the “on” regime above the breakpoint, the emission current density is relatively insensitive to

the exact operating voltage and can be on the order of 1 A per square centimeter of nanotube matrix surface. This high-current density, in addition to the cold-cathode configuration, suggests the nanotube emitters may find uses as micrometer-sized electron beam sources or as pixellated sources for flat panel displays. Any devices utilizing the features of these nanoscaled tubes may benefit from their unique geometry and properties.

#### ACKNOWLEDGMENTS

We thank N. Chopra and C. Piskoti for assistance in nanotube preparation and characterization. This work was supported in part by a UC Berkeley Chancellor’s Initiative Grant, NSF Grant No. DMR-9501156, the U.S. Department of Energy under Contract No. DE-AC03-76SF00098, and by the Office of Naval Research, Order No. N00014-95-F-0099. P.G.C. acknowledges support from a Helmholtz Fellowship. A.Z. received support from the Miller Institute for Basic Research in Science.

- 
- <sup>1</sup>S. Iijima, *Nature* **354**, 56 (1991).  
<sup>2</sup>N. Hamada, S. Sawada, and A. Oshiyama, *Phys. Rev. Lett.* **68**, 1579 (1992).  
<sup>3</sup>J. W. Mintmire, B. I. Dunlap, and C. T. White, *Phys. Rev. Lett.* **68**, 631 (1992).  
<sup>4</sup>M. M. J. Treacy, T. W. Ebbesen, and J. M. Gibson, *Nature* **381**, 678 (1996).  
<sup>5</sup>N. G. Chopra, L. X. Benedict, V. H. Crespi, M. L. Cohen, S. G. Louie, and A. Zettl, *Nature* **377**, 135 (1995).  
<sup>6</sup>L. Langer, V. Bayot, E. Grivei, J.-P. Issi, J. P. Heremans, C. H. Olk, L. Stockman, C. van Haesendonck, and Y. Bruynseraede, *Phys. Rev. Lett.* **76**, 479 (1996).  
<sup>7</sup>T. Guo, P. Nikolaev, A. Thess, D. T. Colbert, and R. E. Smalley, *Chem. Phys. Lett.* **243**, 49 (1995).  
<sup>8</sup>A. G. Rinzler, J. H. Hafner, P. Nikolaev, L. Lou, S. G. Kim, D. Tomanek, P. Nordlander, D. T. Colbert, and R. E. Smalley, *Science* **269**, 1550 (1995).  
<sup>9</sup>W. A. de Heer, A. Chatelain, and D. Ugarte, *Science* **270**, 1179 (1995).  
<sup>10</sup>P. G. Collins and A. Zettl, *Appl. Phys. Lett.* **69**, 1969 (1996).  
<sup>11</sup>T. W. Ebbesen and P. M. Ajayan, *Nature* **358**, 220 (1992).  
<sup>12</sup>R. Gomer, *Field Emission and Field Ionization* (Harvard University Press, Cambridge, 1961), p. 195.  
<sup>13</sup>More exactly,  $E = V/D^*(d/R)$ , where  $D$  is the distance from grid to the planar electrode, but  $d$  is the distance from the grid to the actual emitting tip. In our geometry, the nanotubes extend from the surface  $\leq 1 \mu\text{m}$ , so  $d \approx D \approx 50 \mu\text{m}$  and Eq. (1) results.  
<sup>14</sup>P. G. Collins, A. Zettl, A. Thess, and R. E. Smalley (unpublished).  
<sup>15</sup>J. R. Arthur, *J. Appl. Phys.* **36**, 3221 (1965).  
<sup>16</sup>R. H. Fowler and L. W. Nordheim, *Proc. R. Soc. London Ser. A* **119**, 173 (1928).  
<sup>17</sup>A. Modinos, *Field, Thermionic, and Secondary Electron Emission Spectroscopy* (Plenum, New York, 1984), p. 282.  
<sup>18</sup>W. P. Dyke and W. W. Dolan, *Adv. Electron. Electron Phys.* **8**, 89 (1956).  
<sup>19</sup>L. M. Baskin, O. I. Lvov, and G. N. Furse, *Phys. Status Solidi B* **47**, 49 (1971).  
<sup>20</sup>S. Bajic and R. V. Latham, *J. Phys. D* **21**, 200 (1988).  
<sup>21</sup>S. Bajic and R. V. Latham, *Proceedings of the Second International Conference on Vacuum Microelectronics* (Institute of Physics, Bath, UK, 1989), p. 101.  
<sup>22</sup>R. V. Latham and D. A. Wilson, *J. Phys. D* **16**, 455 (1983).  
<sup>23</sup>L. X. Benedict, V. H. Crespi, S. G. Louie, and M. L. Cohen, *Phys. Rev. B* **52**, 14 935 (1995).  
<sup>24</sup>C. V. Dharmadhikari, R. S. Khairnar, and D. S. Joag, *J. Phys. D* **25**, 125 (1992).  
<sup>25</sup>G. A. J. Amaratunga and S. R. P. Silva, *Appl. Phys. Lett.* **68**, 2529 (1996).  
<sup>26</sup>D. F. Howell, R. D. Groves, R. A. Lee, C. Patel, and H. A. Williams, *Technical Digest of the International Electron Devices Meeting* (IEEE Washington, D.C. 1989), p. 525.  
<sup>27</sup>C. S. Athwal and R. V. Latham, *J. Phys. D* **17**, 1029 (1984).  
<sup>28</sup>V. T. Binh and J. Marien, *Surf. Sci.* **202**, L539 (1988).  
<sup>29</sup>V. T. Binh, S. T. Purcell, G. Gordet, and N. Garcia, *Surf. Sci.* **279**, L197 (1992).